nature communications

Article

https://doi.org/10.1038/s41467-024-53509-6

Early emergence and determinants of human-induced Walker circulation weakening

Received: 21 May 2024

Accepted: 15 October 2024

Published online: 24 October 2024

Check for updates

Mingna Wu[1] ✉, Chao Li[2], Matthew Collins[3], Hongmei Li[2,4], Xiaolong Chen[5], Tianjun Zhou[5,6] & Zhongshi Zhang[1,7] ✉

The Walker circulation is projected to slow down in response to greenhouse gas warming. However, detecting the impact of human activities on changes in the Walker circulation is challenging due to the significant influence of internal variability. Here, based on ensembles of multiple climate models from the Coupled Model Intercomparison Project Phase 6 (CMIP6), we show evidence that the emergence of the human-induced weakening of Walker circulation tends to occur earlier in the middle-upper troposphere than at the surface. This earlier emergence is attributed to a more pronounced initial weakening response of the middle-upper tropospheric Walker circulation to atmospheric CO_2 radiative forcing. We further reveal that the emergence time of a weaker Walker circulation varies across models. This intermodel spread is governed by an ocean thermostat that operates by modulating the zonal sea surface temperature gradient over the tropical Indo-Pacific region. Our findings address the key question of whether and how to detect human-induced large-scale atmospheric circulation changes and provide valuable insights for assessing the associated risks.

The Walker circulation is the most prominent large-scale zonal atmospheric circulation over the tropical Pacific, with warm-moist air rising in the west and cold-dry air descending in the east[1,2]. Changes in the Walker circulation can exert far-reaching impacts throughout the globe, such as shaping the regional hydroclimatic conditions[3–5], regulating the monsoon variations[6–8], and influencing agricultural production and ecosystems[9,10]. As anthropogenic forcing intensifies in the future, detecting and understanding human influences on changes in the Walker circulation emerge as one of the paramount concerns in climate sciences. Underpinning this necessitates determining when and where the human-induced Walker circulation changes will emerge from the large background of internal variability.

The primary focus of studies on the emergence time of climate change signals within the Pacific region is on detecting changes in thermodynamic variables such as temperature and precipitation[11–15], but little attention has been paid to investigating changes in dynamical variables of large-scale circulations. Previous studies found that the mean sea surface temperature (SST) signal emerges earliest in the tropics and can be detected earlier in the western tropical Pacific than the east[11,12,15], while the annual mean rainfall signal over the eastern Pacific is projected to emerge by the mid-21st century[15]. Considering the profound influence of atmospheric circulation in shaping the spatial distributions of temperature, precipitation and wind patterns, ascertaining the emergence of human-induced changes in the Walker circulation is of utmost importance for predicting extreme weather

[1]Department of Atmospheric Science, School of Environmental Studies, China University of Geosciences, Wuhan, China. [2]Max Planck Institute for Meteorology, Hamburg, Germany. [3]Faculty of Environment, Science and Economy, University of Exeter, Exeter, UK. [4]Helmholtz-Zentrum Hereon, Geesthacht, Germany. [5]State Key Laboratory of Numerical Modeling for Atmospheric Sciences and Geophysical Fluid Dynamics (LASG), Institute of Atmospheric Physics, Chinese Academy of Sciences, Beijing, China. [6]University of the Chinese Academy of Sciences, Beijing, China. [7]School of Geographic Science, Nantong University, Nantong, China. ✉e-mail: wumingna@cug.edu.cn; zhongshi.zhang@cug.edu.cn

events like droughts, floods, and tropical cyclones[3,16,17]. However, it remains unclear when the human-induced Walker circulation change will become distinguishable from internal variability, and which factors determine the emergence time of the Walker circulation change.

Accurately estimating the emergence of human-induced Walker circulation changes depends largely on precisely evaluating its intensity changes. Previous studies mainly use indices from low-tropospheric variables, such as sea level pressure (SLP) gradient and surface zonal winds[18–23], to describe the magnitude change in the Walker circulation and uncertainties in its future projections[19,24–26]. However, these low-level indices exhibit a notable concurrence with SST variations[1,27], making it challenging to separate the Walker circulation change signal from SST-driven internal variability. While these low-level indices are widely used, they may not fully capture the complexities of the Walker circulation response to global warming, particularly in the upper troposphere. This is because compared with the lower troposphere, the upper tropical troposphere displays the most substantial intensification of water vapor and temperature warming under the anthropogenic CO_2 forcing[28,29]. This difference in the responses between the upper troposphere and the surface may lead to differing impacts on the Walker circulation at various tropospheric levels[30], resulting in distinct emergence times across these layers. Moreover, while various mechanisms have been proposed to comprehend future changes in the Walker circulation[22,29–35], it is imperative to elucidate which processes actively regulate the emergence of Walker circulation changes.

In this study, we address the question of the emergence of human-induced Walker circulation changes using simulations from Coupled Model Intercomparison Project Phase 6 (CMIP6) models. We use three distinct indices (i.e., dSLP, dW500, and VPmax, see Methods) from the low-level to the middle and upper troposphere to describe the intensity of the Walker circulation. Based on these indices, we determine the time of emergence (ToE) of Walker circulation changes at different tropospheric levels, identify the multimodel-based consensus, and investigate the origin of intermodel discrepancies. We demonstrate that the ToE of the Walker circulation weakening potentially occurs earlier in the middle-upper troposphere than at the surface. An earlier ToE is also more evident in models that exhibit a stronger weakening of the zonal SST gradient after a long-term adjustment to CO_2 increase.

Results

Future Walker circulation responses on different levels

The Walker circulation is projected to weaken at different tropospheric levels in a warmer future climate (Fig. 1). At the surface, an increase in low SLP over the Indo-Pacific warm pool reduces the east-west SLP gradient (Fig. 1a, b). In the middle and upper troposphere, positive trends over the western Pacific (in regions of climatological ascent) and negative trends over the eastern Pacific (in regions of climatological descent) indicate a weakening of both ascending and descending motions of the Walker circulation (Fig. 1c–f). This weakening is further supported by trends in vertical velocity, with positive values in the western Pacific and negative values in the eastern Pacific (Fig. 1g, h).

Almost all models project an overall weakening of the Walker circulation under both medium and high greenhouse gas emission scenarios based on different indices (Supplementary Fig. 1). However, changes in the Walker circulation exhibit remarkably multidecadal variations due to internal variability (Supplementary Fig. 1a, c, and e). After removing the influence of internal variability (see Methods), the externally forced signal shows a weakening trend of Walker circulation at different tropospheric levels in response to global warming (Supplementary Fig. 1b, d, f). This forced weakening happens with enhanced warming in the eastern tropical Pacific (Supplementary Fig. 2c, d) and a greater rise in the tropical mean upper tropospheric temperature (Supplementary Fig. 2e, f).

ToE of the Walker circulation change

The temporal evolution of signal-to-noise ratio (see Methods) reveals that the forced Walker circulation change is detected earlier in the middle and upper troposphere than in the lower troposphere (Fig. 2a, c and e). Under the SSP5-8.5 scenario, the multimodel ensemble mean of the forced signal is likely to exceed the range of internal variability in 2040s in the dW500 index (middle troposphere) and 2050s in the VPmax index (upper troposphere) (Fig. 2c and e), while it will not emerge until the 2080s in the dSLP index (lower troposphere) (Fig. 2a). The forced weakening of Walker circulation under the SSP2-4.5 scenario shows similar results, but with a delayed emergence period across all tropospheric levels (Fig. 2a, c and e). Moreover, there is a spread in the signal-to-noise ratio across models, gradually increasing over time (Fig. 2a, c, and e). This increased intermodel spread is explained by the increased intermodel uncertainty in the forced signal of the Walker circulation change (Supplementary Fig. 1b, d, and f).

The ToE analysis (see Methods) further confirms a higher detectability of the Walker circulation weakening in the middle and upper troposphere (Fig. 2b, d, and f). A majority of climate models (93% and 83%) exhibit detectable weakening of the Walker circulation by the end of this century based on the middle and upper tropospheric indices under the SSP5-8.5 scenario (Fig. 2d and f), whereas only approximately half of the models (53%) demonstrate detectability based on the low-level index (Fig. 2b). Furthermore, the ensemble-mean ToE appears earlier in the middle and upper troposphere (year 2050 and year 2053) compared to that at the surface (year 2070) (Supplementary Fig. 3b, d, and f). Earlier emergence of the Walker circulation weakening in the middle-upper troposphere is also found under the SSP2-4.5 scenario, but the ToE is later than that under the SSP5-8.5 scenario in models by several decades (Fig. 2b, d, f).

Factors contributing to early ToE in the middle-upper troposphere

The varying emergence time in the Walker circulation weakening at different tropospheric levels is largely attributed to the distinct signal-to-noise ratio of the Walker circulation change in response to CO_2 forcing. The signal of a weaker Walker circulation emerges earliest in the middle troposphere, while it is delayed by about 30 years at the surface (Fig. 3a, c, and e). In the abrupt4×CO_2 experiment, the signal-to-noise ratio indicated by the dSLP index is of smaller magnitude compared to that of the dW500 and VPmax indices (Fig. 3a, c, and e). This lower signal-to-noise ratio for the dSLP index results in a longer time required for the signal to exceed the noise range. Consequently, the signal in the dSLP index does not surpass the noise until about 30 years later, whereas in the dW500 and VPmax indices, the signal of a weaker Walker circulation emerges much earlier (Fig. 3a, c, and e).

The spatial distribution differences in both signal magnitude and internal variability explain the variation in emergence times among the indices. At the surface, the SLP signal only emerges in the western tropical Pacific in the first 10 years of the abrupt4×CO_2 experiment (Fig. 4a). This is because the SLP strengthens over the western tropical Pacific in response to increased CO_2 forcing in the first few years, with no significant change seen in the eastern tropical Indian Ocean and eastern tropical Pacific (Supplementary Fig. 4a). However, the internal variability in the latter regions is higher than that in the western tropical Pacific (Supplementary Fig. 4b). Consequently, the signal-to-noise ratio peaks in the western tropical Pacific. Therefore, the difference between the east and the west over the tropical Pacific yields a low signal-to-noise ratio in the dSLP index. In contrast, the dW500 index emerges earliest due to a stronger signal in the Maritime Continent region and the central tropical Pacific, coupled with lower internal variability in these areas (Fig. 4c, d and Supplementary Fig. 4c, d).

The stronger signal in the middle-upper troposphere is related to a larger fast weakening response in the middle-upper component of

https://doi.org/10.1038/s41467-024-53509-6

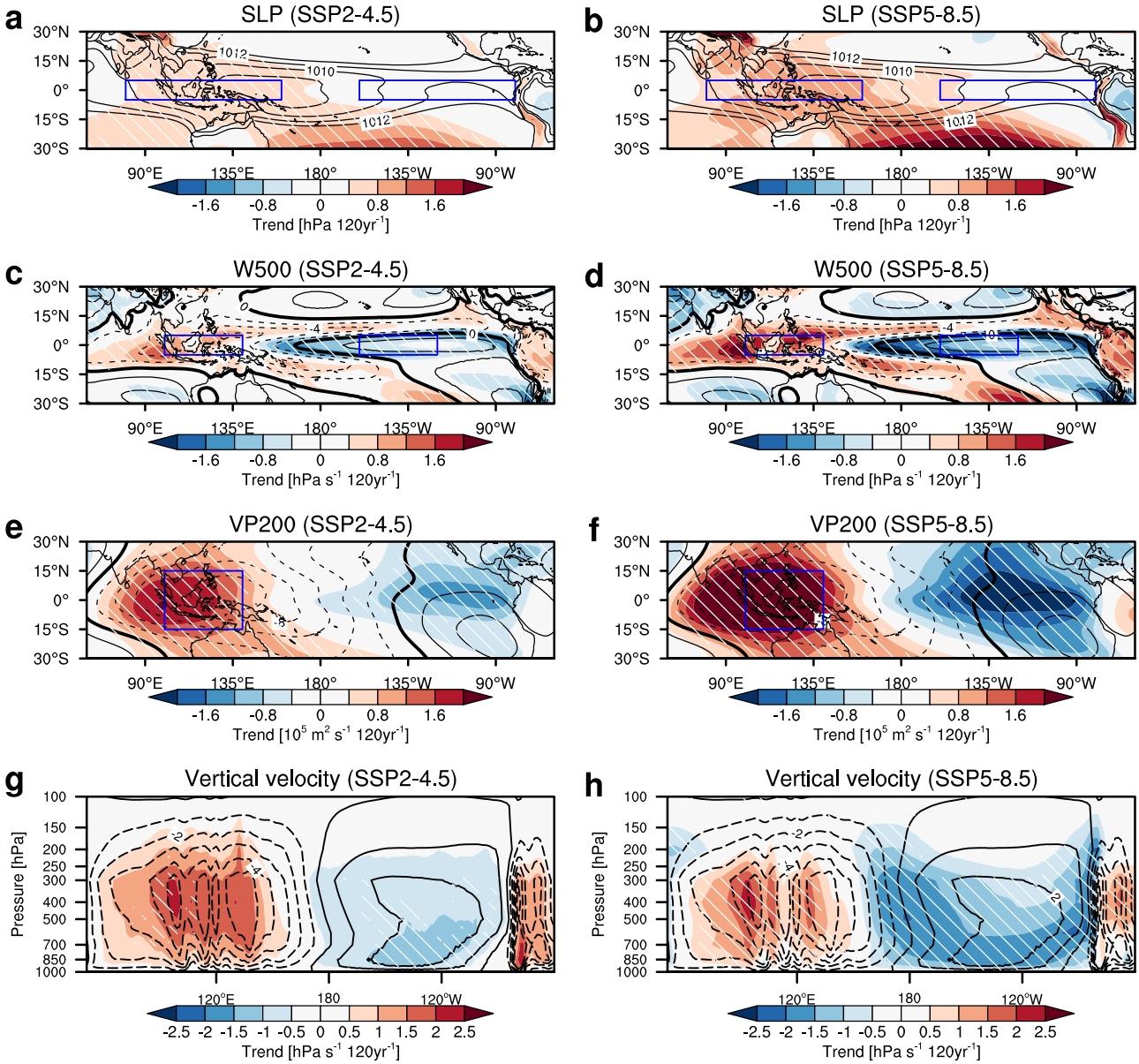

Fig. 1 | Long-term changes in the Walker circulation for 1980–2099 under different emission scenarios. Spatial distribution of linear trends in (**a**) sea level pressure, (**c**) vertical velocity at 500 hPa (positive values refer to downward velocity), (**e**) velocity potential at 200 hPa, and (**g**) area-averaged vertical velocity over 5°S–5°N under the SSP2-4.5 scenario. Black contours denote the climatological mean from 1980–2014. White slant hatchings denote areas where more than 80% of the models agree in sign of the trends. **b**, **d**, **f** and **h** are the same as (**a**), (**c**), (**e**), and (**g**) but under the SSP5-8.5 scenario. Boxes in (**a**–**f**) indicate regions used to define the Walker circulation intensity indices and the zonal SST gradient (see Methods).

the Walker circulation in response to CO_2 forcing. The temporal evolution of the Walker circulation response in all indices from the abrupt4×CO_2 experiment shows two different stages: a fast response, which refers to the response in the first few years to the abruptly imposed CO_2, and a slow response, which is characterized by a longer-term adjustment (Fig. 3b, d, and f). The slow responses in all three indices display a pronounced weakening of the Walker circulation, which stabilizes after about 100 years (Fig. 3b, d, and f). However, the fast response in the surface differs from that in the middle-upper troposphere. At the surface, the weakening of the Walker circulation becomes significant after 20–30 years, while in the middle-upper troposphere, the Walker circulation weakens from the initial stage (Fig. 3b, d, and f).

The larger fast weakening of the middle and upper Walker circulation is caused by stronger radiative forcing, enhanced static stability, and slower radiative cooling in the middle and upper troposphere compared to the surface. The increased atmospheric CO_2 concentration reduces infrared radiation loss more in the upper troposphere than at the surface, leading to faster warming and greater static stability at higher altitudes[31,36,37]. This enhanced stability weakens the middle and upper Walker circulation, as the upper troposphere stabilizes more rapidly than the lower layers[36,37]. As the entire troposphere warms, the moist adiabatic lapse rate disproportionately increases static stability in the upper troposphere, further suppressing buoyancy-driven motions that support the Walker circulation[36,38–40]. Additionally, CO_2-driven warming slows the rate of radiative cooling[31,37–39], weakening vertical motions in the middle and upper troposphere, leading to a significant weakening of the Walker circulation at these levels[37,39]. In contrast, the circulation changes near the surface are primarily influenced by boundary layer processes and surface fluxes, which are closely tied to SST changes. Hence, when the zonal SST gradient begins to decrease after about 30 years, the SLP

https://doi.org/10.1038/s41467-024-53509-6

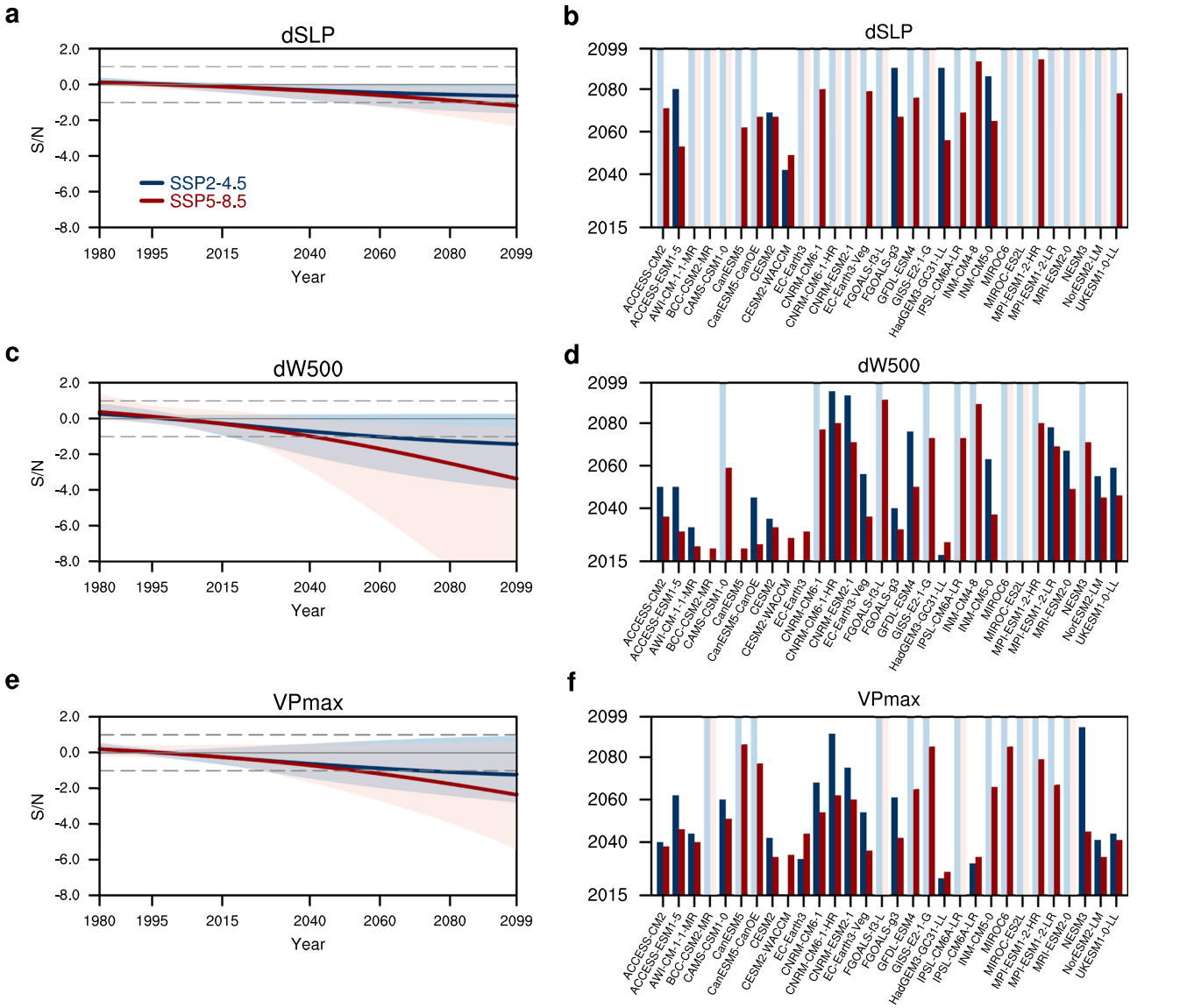

Fig. 2 | Comparison of detectability of the Walker circulation intensity change at different tropospheric levels. a Signal-to-noise ratio of the Walker circulation intensity change relative to the 1980–2014 baseline calculated based on the sea-level pressure gradient (dSLP). Blue (red) thick line denotes the ensemble mean of models under the SSP2-4.5 (SSP5-8.5) scenario, while blue (red) shading indicates the model spread. The gray dashed lines denote the signal-to-noise ratio of 1 or -1. **b** Time of emergence (ToE) for annual-mean Walker circulation intensity change based on the dSLP index, under the SSP2-4.5 (blue bars) and SSP5-8.5 (red bars) scenarios. Lighter blue and red bars indicate models in which no emergence of the forced Walker circulation intensity change is detected by the end of the 21st century for the respective scenarios. **c**–**f** are the same as (**a**–**b**) but based on the 500 hPa vertical velocity gradient (dW500) and the maximum absolute value in the 200 hPa velocity potential over the western tropical Pacific (VPmax), respectively.

also starts to change (Supplementary Fig. 5). The above results suggest that the mid-to-upper-level component of the Walker circulation weakens directly in response to increased atmospheric CO_2 radiative forcing[36], while the weakening of its surface manifestation is delayed by SST adjustment processes related to ocean dynamics. Therefore, the forced signal in Walker circulation change indicated by indices from the middle and upper troposphere is more likely to be detected earlier than the lower tropospheric indices.

Sources of intermodel uncertainty in ToE

A large spread exists in the ToE across different models (Fig. 2 and Supplementary Fig. 3). For models exhibiting ToE before 2099, the year of ToE displays a wide-ranging distribution exceeding 50 years (Supplementary Fig. 3). Specifically, the ToE shows a range of 2049–2094 (2042–2090) in the dSLP index, 2021–2091 (2015–2095) in the dW500 index, and 2026–2086 (2015–2094) in the VPmax index under the SSP5-8.5 (SSP2-4.5) scenario (Supplementary Fig. 3). Notably, certain models even indicate the absence of the Walker circulation weakening emergence (Fig. 2b, d and f).

The intermodal uncertainty in ToE likely stems from a wide range of forced signals and internal variability across different models. To analyze the source of intermodel uncertainty in the ToE, we calculate the ToE by simultaneously considering the forced signal and internal variability in all the models based on three indices (Fig. 5a, c, and e). Here we estimate the magnitude of the forced signal as the long-term trend of the forced Walker circulation change. The results show that the ToE is influenced by both internal variability and the forced signal, with an earlier ToE appearing when there is smaller internal variability and a larger forced signal (Fig. 5a, c, e and Supplementary Fig. 6a, c and e). Since the Walker circulation responds to CO_2 forcing with both a fast and slow response, we examine the intermodel relationships between ToE and the fast response (Supplementary Fig. 7), ToE and the

https://doi.org/10.1038/s41467-024-53509-6

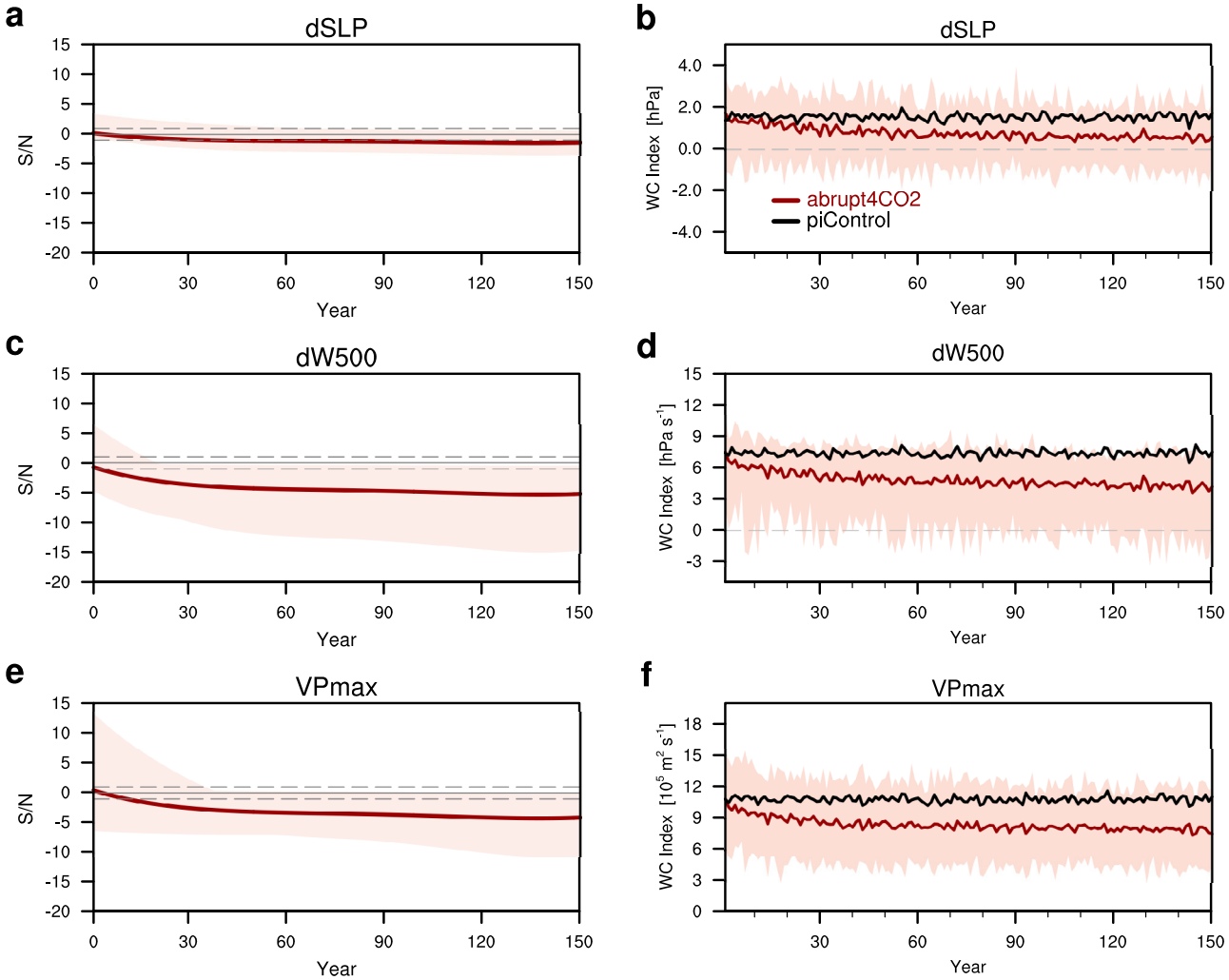

Fig. 3 | Time evolution of the signal-to-noise ratio and the intensity of Walker circulation in the abrupt4×CO_2 experiment. a, **c** and **e** Time series of the signal-to-noise ratio of the Walker circulation change in the abrupt4×CO_2 experiment based on the sea-level pressure gradient (dSLP), the 500 hPa vertical velocity gradient (dW500), and the maximum absolute value in the 200 hPa velocity potential (VPmax), respectively. **b**, **d** and **f** Time series of the Walker circulation intensity in the pre-industrial control experiment (black line) and the abrupt4×CO_2 experiment (red line) based on dSLP, dW500, and VPmax indices, respectively. Red shading indicates the model spread in the abrupt4×CO_2 experiment.

slow response (Fig. 5b, d, f and Supplementary Fig. 6b, d and f), and ToE and internal variability (Supplementary Fig. 8). The highest inter-model correlation coefficient between the ToE and the slow response suggests the major role of slow response in explaining the intermodel difference of ToE (Fig. 5b, d, f, and Supplementary Fig. 6b, d and f). The stronger the slow response is, the earlier the ToE appears, and vice versa. For models showing Walker circulation weakening but no emergence (Fig. 2b, d, f), this can be attributed to a smaller slow response rather than larger internal variability (Fig. 5 and Supplementary Fig. 8).

The slow response of the Walker circulation change is mainly determined by zonal SST gradient change (Supplementary Fig. 9), which is modulated by an ocean thermostat response. We select two subsets of models, namely Group-E (models with an earlier ToE) and Group-L (models with a later ToE), based on the occurrence time of the ToE to verify the influence of the ocean thermostat mechanism (Table S1) (see Methods). Models in Group-E show earlier ToE in all three indices while ToE in Group-L models arises later. In Group-L models, the initial SST change over the first 10 years resembles the ocean thermostat response, displaying negative SST anomalies in the central equatorial Pacific (Fig. 6a). It shows that an enhanced upwelling of cold water acts as a balancing mechanism to counter the radiative forcing caused by increased CO_2[33–35]. The cooling or suppressed warming pattern eventually shifts to an enhanced eastern equatorial Pacific warming (Fig. 6b). In Group-E models, however, immediate warming over the eastern equatorial Pacific occurs, which progressively intensifies over time (Fig. 6c, d). The results above suggest that the ocean thermostat delays the weakening of the zonal SST gradient. The transition from cooling to warming SST pattern in Group-L models delays the weakening of the Walker circulation, thus postponing the emergence of a weaker Walker circulation. However, the enhanced extratropical warming and weakened subtropical oceanic cells diminish the supply of cold water to equatorial upwelling after a longer-term of adjustment in both groups of models, resulting in a reduced zonal SST gradient[30]. Therefore, the difference in the magnitude of the slow response in the zonal SST gradient across models leads to intermodel uncertainty in the slow response of the Walker circulation to CO_2 forcing, and consequently, in the ToE.

Discussion

We have investigated the emergence time of the Walker circulation change based on three intensity indices within the CMIP6 models. We find that the human-induced weakening of the Walker circulation is

https://doi.org/10.1038/s41467-024-53509-6

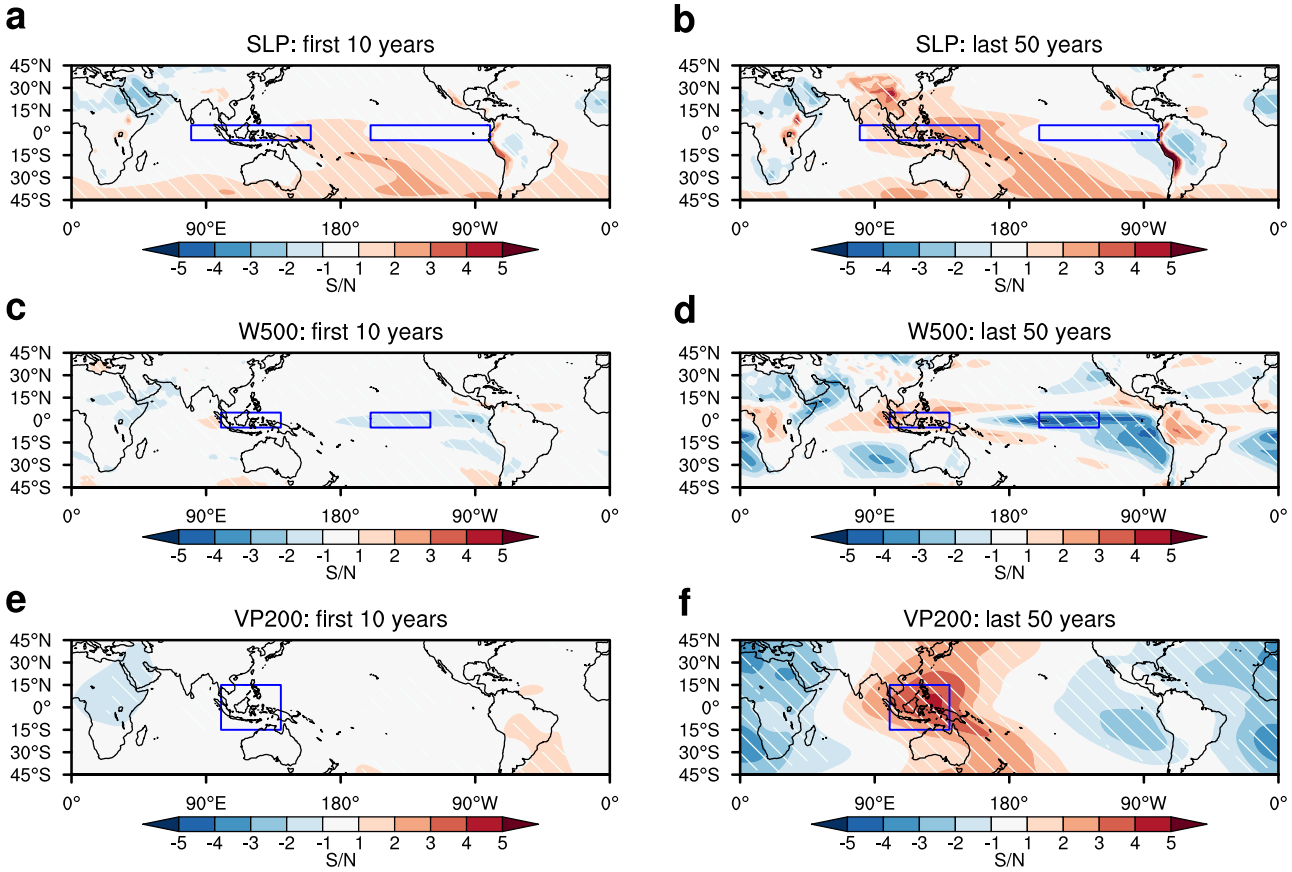

Fig. 4 | Signal-to-noise ratio of the Walker circulation change in response to CO_2 forcing at different tropospheric levels in the abrupt4×CO_2 experiment. **a**–**b** Spatial distribution of the signal-to-noise ratio of sea level pressure (SLP) for the first 10 years and the last 50 years. Shown are the multimodel ensemble mean. White slant hatchings denote areas where more than 80% of the models agree on the sign of changes. **c**–**f** are the same as (**a**–**b**) but for vertical velocity at 500 hPa (W500) and velocity potential at 200 hPa (VP200), respectively. Boxes indicate regions used to define the Walker circulation intensity indices.

more likely to be detected in the middle and upper troposphere than in the lower levels. We emphasize that the earlier ToE in the middle and upper troposphere is due to both statistical and physical factors. The ToE is determined by the signal-to-noise ratio, which depends on both the magnitude of the signal and the noise. The signal-to-noise ratio indicated by the surface index is smaller compared to that of the mid- and upper-level indices, resulting in a longer time required for the signal to exceed the threshold. Moreover, in addition to the El Niño-like warming over the eastern tropical Pacific, the temperature response to increasing CO_2 concentrations also includes a significant warming of the tropical upper troposphere. This distinct three-dimensional spatial pattern in temperature changes contributes to the weakening of the Walker circulation. Because climate models exhibit higher certainty in projecting the increase in tropical mean upper tropospheric temperature compared to changes in the zonal SST gradient, the forced signal of Walker circulation change—reflected in middle and upper troposphere variables—is more robust and thus more likely to be detected earlier than signals derived from lower tropospheric variables. This underscores the need for greater focus on middle and upper tropospheric variables for early detection of human-induced changes in tropical large-scale atmospheric circulations. While all the indices are physically consistent and provide valuable insights, we suggest prioritizing those from the middle and upper troposphere for detecting Walker circulation changes under global warming, as they present the earliest signal. Our extensive investigation into the uncertainty across models suggests that the intermodel spread in the emergence time originates from the uncertainty in the slow response of Walker circulation to CO_2 forcing. Models that exhibit a stronger slow weakening of the Walker circulation tend to have an earlier ToE, and vice versa. The findings provide a physical basis for reducing the uncertainty in the emergence of tropical large-scale circulation change signals in CMIP6 models, contributing to a more accurate assessment of the relevant impacts.

Our results demonstrate the emergence of a human-induced Walker circulation weakening. However, it has been widely noticed that the observed Walker circulation has exhibited a robust strengthening over the past few decades[19,20,23,24,26,41–49]. This observed strengthening is accompanied by a La Niña-like cooling trend over the tropical eastern Pacific[19,23,43,50–52], which plays a dominant role in driving the enhancement of Walker circulation strength[52,53]. Recently, Heede and Federov[52] proposed that the observed SST cooling trends over the tropical eastern Pacific are results of three processes, i.e., the globally uniform warming trend, the negative PDO/IPO phase, and the warming in Northern Hemisphere/Indo-West Pacific. The first two signals represent the effects of global warming and internal variability, respectively, whereas the third signal indicates the fast ocean thermostat-like response to global warming[34,52].

To compare our results with those from Heede and Federov[34], we select the same four models that demonstrate the La Niña-like fast changes (namely ACCESS-CM2, CNRM-ESM2-1, CNRM-CM6-1-HR, and MPI-ESM1-2-LR) to examine the associated Walker circulation response. We find a fast increase in SLP gradient during the first 10 years in these models (Supplementary Fig. 10a), indicating the fast strengthening of the Walker circulation at the surface. However, at middle and upper levels, there are notable positive anomalies in the tropical western Pacific and eastern Indian Ocean, accompanied by

https://doi.org/10.1038/s41467-024-53509-6

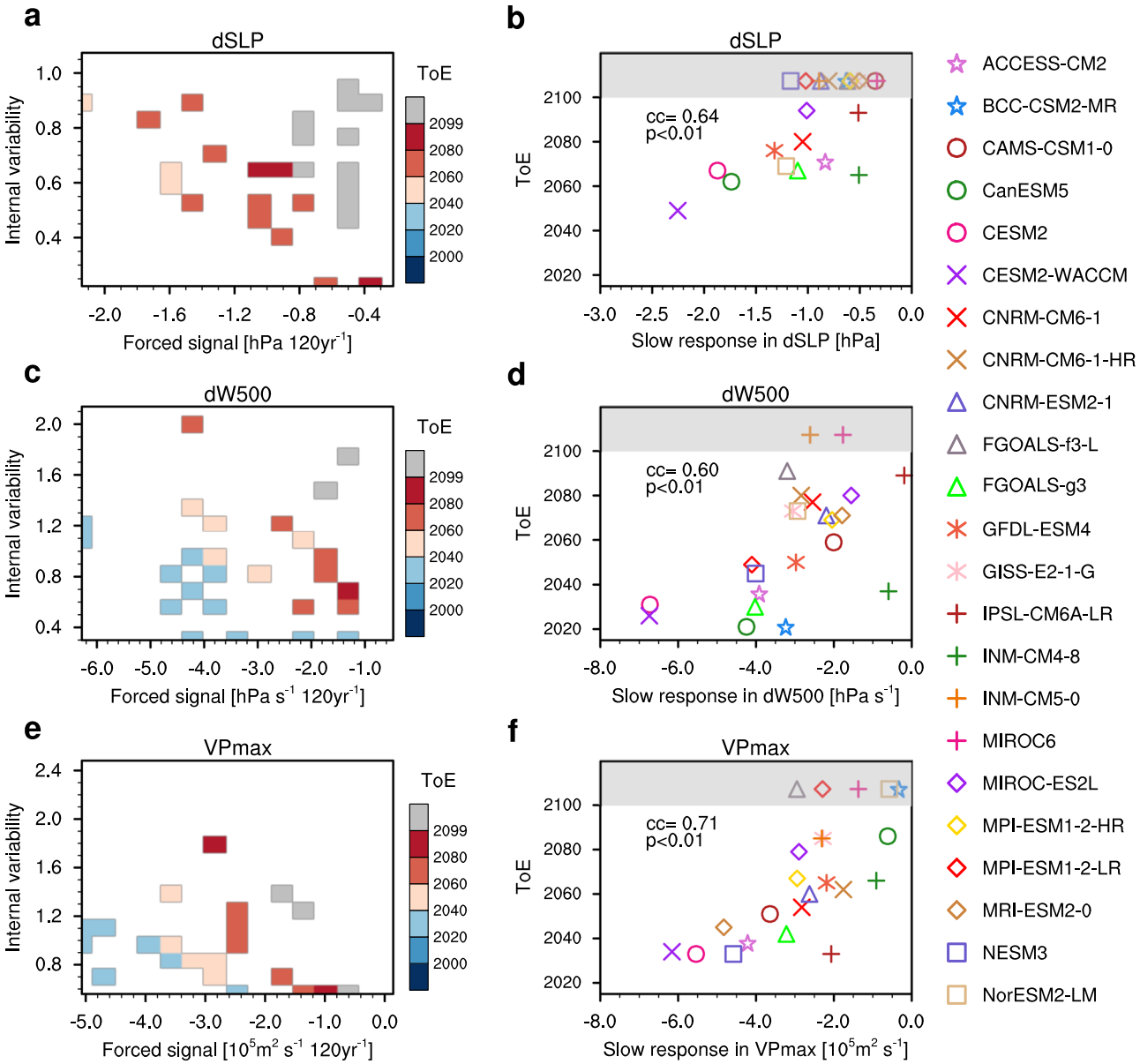

Fig. 5 | Sources of uncertainty in ToE for the Walker circulation change. a Likely range of time of emergence (ToE) determined by forced signal (*x*-axis) and internal variability (*y*-axis) based on sea-level pressure gradient (dSLP) in CMIP6 models under the SSP5-8.5 scenario. **b** Intermodel relationship between ToE and slow response of the Walker circulation (See Methods) in the abrupt4×CO_2 experiment based on the dSLP index. The intermodel correlation coefficient and *p*-value are shown in the upper-left corner of the panels, with $p < 0.01$ denoting a significant correlation. **c**–**f** are the same as (**a**–**b**) but for the 500 hPa vertical velocity gradient (dW500) and the maximum absolute value in the 200-hPa velocity potential over the western tropical Pacific (VPmax), respectively. Gray shading in (**b**), (**d**) and (**f**) indicates models without ToE.

negative anomalies in the tropical eastern Pacific (Supplementary Fig. 10c and e). These anomalies signify a weakening of upward motion in the west and downward motion in the east, which progressively intensifies over time (Supplementary Fig. 10d and f). This result suggests that even in models exhibiting a La Niña-like fast response, the middle and upper component of the Walker circulation weakens significantly from the initial stage. We further analyze the timescales of the correlation coefficients between the zonal SST gradient and different Walker circulation indices to determine when the zonal SST gradient can exert stable impacts on the middle and upper troposphere (Supplementary Fig. 11). The results show that after about 50 years, the correlation between the zonal SST gradient and the middle and upper indices stabilizes at a high level, while its correlation with the surface index remains consistently the highest across all timescales.

The above results further reinforce our main conclusion that the emergence of the Walker circulation weakening can be detected earlier in the middle-upper tropospheric levels. As CO_2 forcing continues to rise, the fast response will eventually transit into a slow response characterized by an El Niño-like warming and a weakened Walker circulation[30,53,54]. Moreover, the PDO/IPO is likely to shift its phase from negative to positive in the next few years[23], which will weaken the zonal SST gradient hence the Walker circulation. Therefore, it is likely that the observed Walker circulation strengthening will not last long and will weaken in the future in response to increased CO_2 forcing. In light of these findings, there is a strong possibility of observing the emergence of a human-induced Walker circulation weakening in the future.

Another notable issue is that current climate models fail to replicate the recent Walker circulation strengthening in observations[19,23,41,50]. This long-standing conundrum has brought the

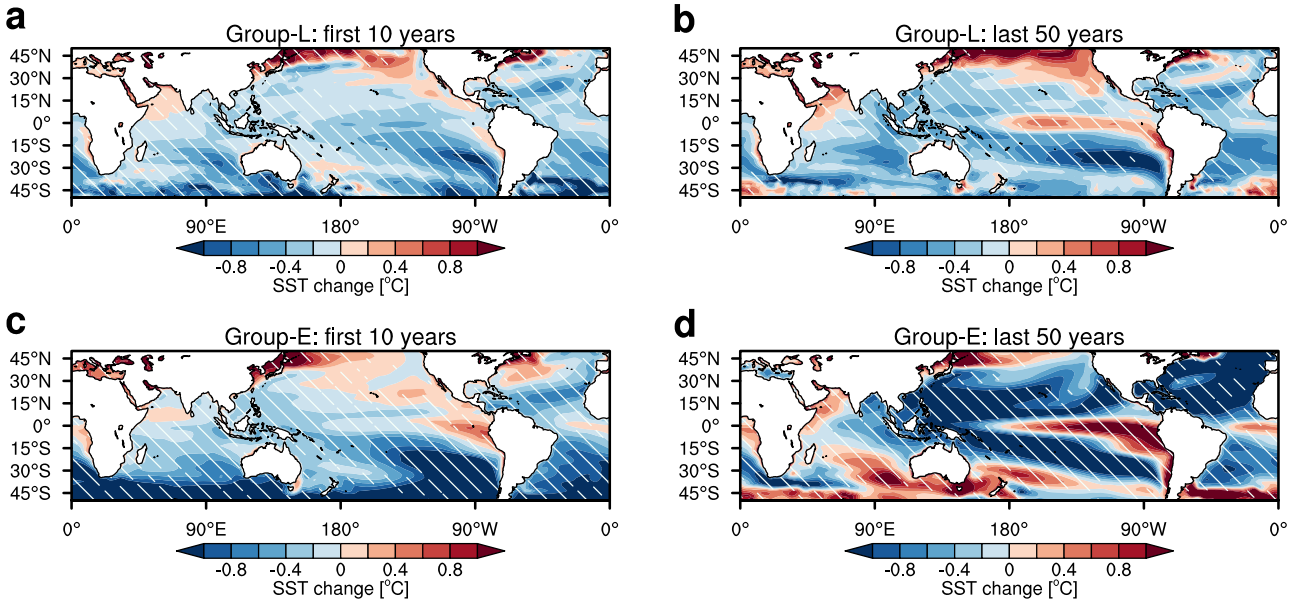

Fig. 6 | Verifying the role of the ocean thermostat mechanism. a Initial and (**b**) long-term sea surface temperature (SST) anomaly patterns in the abrupt4×CO_2 experiments for Group-L models. **c**–**d** The same as (**a**–**b**) but for Group-E models. The SST anomalies are derived by comparing them to the piControl experiments and then subtracting the average ocean warming within the 40°S–40°N, 60°E–60°W region. Shown are the ensemble mean. White slant hatchings denote areas where all the models agree in sign.

robustness of the future projection of a weaker Walker circulation into question. This discrepancy arises from several factors, including internal variability, potential underestimation of the forced response to external forcings, and model errors[55]. Internal variability, particularly modes like the PDO and IPO, has significantly contributed to the observed strengthening of the Walker circulation in recent decades[19,23,50]. Models often struggle to accurately represent this internal variability[23], leading to discrepancies between observed and modeled Walker circulation changes. Moreover, models may potentially underestimate the forced response, such as the fast strengthening response of the Walker circulation to global warming[34,52]. Additionally, model errors in simulating the tropical Pacific[35] or Atlantic ocean[20] mean states and the subtropical cloud feedback[56] may contribute to this discrepancy by underestimating inter-basin interactions and the effects of Southern Ocean cooling[54]. Considering all the factors mentioned above, we acknowledge that the actual emergence time of Walker circulation weakening may occur later than projected by models, but first be detected in the middle and upper troposphere.

Finally, we note that some factors may accelerate the emergence of the weakening of Walker circulation. For example, the amplitude of ENSO is proposed to increase by the end of the century[57,58], potentially exacerbating the weakening of the Walker circulation and hastening the emergence time of the weakening signal. Additionally, since aerosols typically delay the onset of warming in the eastern equatorial Pacific[34], the expected reduction in anthropogenic aerosols may also accelerate the emergence of a weakened Walker circulation under future emissions reduction policies.

Methods

Model simulations

CMIP6 model simulations. Monthly outputs from 30 CMIP6 models are used in this study (Table S1). The historical runs for 1980–2014 and the future projections under the SSP2-4.5 and SSP5-8.5 scenarios for 2015–2099 are analyzed. The SSP2-4.5 scenario represents a moderate-emission pathway, with a projected radiative forcing of 4.5 W/m² by 2100. In contrast, the SSP5-8.5 scenario reflects a high-emission, fossil fuel-reliant pathway, leading to a radiative forcing of 8.5 W/m² by 2100[59].

We also use 24 models with 150 years simulations from the piControl experiment and abrupt4×CO_2 rise experiment to investigate the response of Walker circulation to CO_2 forcing. The piControl experiment simulates pre-industrial conditions, representing the period before large-scale industrialization. In the abrupt4×CO_2 experiment, the CO_2 concentration is immediately and abruptly quadrupled from the global annual mean 1850 value, allowing for the assessment of radiative forcing caused by elevated atmospheric CO_2 levels[60].

A 35 year period from 1980–2014 is defined as the reference period and all changes under global warming are calculated relative to this reference period in historical and future SSP scenarios. The global mean surface air temperature (GSAT) increase is computed using the near-surface air temperature measured at 2 meters, based on historical experiments, relative to the period of 1851–1910. Additionally, we use the 150 year period from the piControl experiments as the reference period for the abrupt4×CO_2 experiments. One ensemble realization per model is used to give equal weights to each model and all the model outputs are bilinearly interpolated into a 1.5° × 1.5° grid before analyses.

Statistical analysis

Indices for Walker circulation intensity. Here we mainly focus on the annual-mean change of the Walker circulation. We use three indices at different levels to estimate the intensity of the Walker circulation: the sea-level pressure gradient (dSLP), the vertical velocity gradient at 500hPa (dW500), and the maximum velocity potential at 200 hPa (VPmax). The dSLP is one of the most commonly used index tightly linked to SST gradient, which is defined as the sea-level pressure anomaly difference between the eastern (5°S–5°N, 160°–80°W) and western (5°S–5°N, 80°–160°E) tropical Pacific[22]. The dW500 describes the vertical motion in the ascending and descending branches of the Walker circulation, which is defined as the vertical velocity anomaly difference at 500hPa between the Maritime Continent region (5°S–5°N, 160°–120°W) and central tropical Pacific (5°S–5°N, 100°–140°E)[25]. The VPmax index is defined as the maximum absolute value over 15°S–15°N, 100°–140°E in the deviation from the zonal mean for velocity potential at 200 hPa, which reflects the characteristic of the circulation in the upper troposphere[25].

Estimating the signal of the Walker circulation change

The signal of modeled annual-mean change in the Walker circulation is extracted by calculating the response of Walker circulation to global warming[11,15]. To obtain the global warming signal, we first calculate the time series of GSAT relative to the pre-industrial period 1851–1910 ($T(t)$) (Supplementary Fig. 2a). We then apply a fourth order polynomial to $T(t)$ to smooth the global warming time series, which can be written as $\widetilde{T}(t)$ (Supplementary Fig. 2b). Hence, the signal of Walker circulation change, $S(t)$, can be obtained by regressing the annual-mean Walker circulation change onto $\widetilde{T}(t)$:

$$S(t) = a\widetilde{T}(t) + b \quad (1)$$

where a is the regression coefficient representing the sensitivity of Walker circulation to global warming, while b represents the intercept.

ToE of Walker circulation change

The ToE of Walker circulation change is defined as the first year when the signal-to-noise ratio (S/N) becomes larger (smaller) than 1 (−1) and continues into the future if the Walker circulation strengthens (weakens) in response to global warming. The N is computed as the standard deviation of the anomaly for annual-mean Walker circulation index for the period 1851–1910, when the anthropogenic forcing was much smaller than present[13].

Definition of fast and slow response

To isolate the response of Walker circulation to CO_2 forcing, we compare changes in different variables from abrupt4×CO_2 experiments with that in the pre-industrial control (piControl) experiments[30]. We define the fast response as the mean of changes during the first 10 years, from year 1 to year 10, after imposed forcing. The slow response is defined as the mean of changes in the last 50 years. Hence, the strengthening and weakening of the Walker circulation in abrupt4×CO_2 experiment refers to a stronger or weaker Walker circulation relative to the piControl experiment.

Selection of Group-E and Group-L models

Here we categorize models into Group-E and Group-L based on the timing of ToE occurrence across all three indices. Group-E consists of the top 30% of models where ToE appears earliest across all indices, while Group-L comprises the bottom 30% of models where ToE appears latest.

Data availability

The monthly outputs from CMIP6 models are available from the following website: https://esgf-node.llnl.gov/search/cmip6/.

Code availability

The data in this study is analyzed with NCAR Command Language (NCL; http://www.ncl.ucar.edu/). All relevant codes used in this work are available, upon reasonable request, from the corresponding author M.W.

References

1. Bjerknes, J. Atmospheric teleconnections from the equatorial Pacific. *Mon. Weather Rev.* **97**, 163–172 (1969).
2. Julian, P. R. & Chervinc, R. M. A study of the southern oscillation and Walker circulation phenomenon. *Mon. Weather Rev.* **106**, 1433–1451 (1978).
3. Espinoza, J. C., Segura, H., Ronchail, J., Drapeau, G. & Gutierrez-Cori, O. Evolution of wet-day and dry-day frequency in the western amazon basin: relationship with atmospheric circulation and impacts on vegetation. *Water Resour. Res.* **52**, 8546–8560 (2016).
4. van der Lubbe, H. J. L. et al. Indo-Pacific Walker circulation drove pleistocene African aridification. *Nature* **598**, 618–623 (2021).
5. Zhao, S. & Cook, K. H. Influence of walker circulations on East African rainfall. *Clim. Dyn.* **56**, 2127–2147 (2021).
6. Huang, X. et al. The recent decline and recovery of indian summer monsoon rainfall: relative roles of external forcing and internal variability. *J. Clim.* **33**, 5035–5060 (2020).
7. Wang, B., Liu, J., Kim, H.-J., Webster, P. J. & Yim, S.-Y. Recent change of the global monsoon precipitation (1979–2008). *Clim. Dyn.* **39**, 1123–1135 (2011).
8. Webster, P. J. et al. Monsoons: Processes, predictability, and the prospects for prediction. *J. Geophys. Res.: Oceans* **103**, 14451–14510 (1998).
9. Holmgren, M., Scheffer, M., Ezcurra, E., Gutiérrez, J. R. & Mohren, G. M. J. El Niño effects on the dynamics of terrestrial ecosystems. *Trends Ecol. Evol.* **16**, 89–94 (2001).
10. Phillips, J. G., Cane, M. A. & Rosenzweig, C. ENSO, seasonal rainfall patterns and simulated maize yield variability in Zimbabwe. *Agric. Meteorol.* **90**, 39–50 (1998).
11. Hawkins, E. & Sutton, R. Time of emergence of climate signals. *Geophys. Res. Lett.* **39**, L01702 (2012).
12. Mora, C. et al. The projected timing of climate departure from recent variability. *Nature* **502**, 183–187 (2013).
13. Park, C.-E. et al. Keeping global warming within 1.5 °C constrains emergence of aridification. *Nat. Clim. Change* **8**, 70–74 (2018).
14. Rojas, M., Lambert, F., Ramirez-Villegas, J. & Challinor, A. J. Emergence of robust precipitation changes across crop production areas in the 21st century. *Proc. Natl Acad. Sci. USA.* **116**, 6673–6678 (2019).
15. Ying, J. et al. Emergence of climate change in the tropical Pacific. *Nat. Clim. Change* **12**, 356–364 (2022).
16. Marengo, J. A. & Espinoza, J. C. Extreme seasonal droughts and floods in Amazonia: causes, trends and impacts. *Int. J. Climatol.* **36**, 1033–1050 (2016).
17. Wang, X. & Liu, H. PDO modulation of ENSO effect on tropical cyclone rapid intensification in the western North Pacific. *Clim. Dyn.* **46**, 15–28 (2015).
18. Bayr, T., Dommenget, D., Martin, T. & Power, S. B. The eastward shift of the Walker circulation in response to global warming and its relationship to ENSO variability. *Clim. Dyn.* **43**, 2747–2763 (2014).
19. England, M. H. et al. Recent intensification of wind-driven circulation in the Pacific and the ongoing warming hiatus. *Nat. Clim. Change* **4**, 222–227 (2014).
20. McGregor, S. et al. Recent Walker circulation strengthening and Pacific cooling amplified by Atlantic warming. *Nat. Clim. Change* **4**, 888–892 (2014).
21. Tanaka, H. L., Ishizaki, N. & Kitoh, A. Trend and interannual variability of Walker, monsoon and Hadley circulations defined by velocity potential in the upper troposphere. *Tellus* **56**, 250–269 (2004).
22. Vecchi, G. A. et al. Weakening of tropical Pacific atmospheric circulation due to anthropogenic forcing. *Nature* **441**, 73–76 (2006).
23. Wu, M. et al. A very likely weakening of Pacific Walker circulation in constrained near-future projections. *Nat. Commun.* **12**, 6502 (2021).
24. Ma, S. & Zhou, T. Robust strengthening and westward shift of the tropical Pacific Walker circulation during 1979–2012: a comparison of 7 sets of reanalysis data and 26 CMIP5 models. *J. Clim.* **29**, 3097–3118 (2016).
25. Plesca, E., Grützun, V. & Buehler, S. A. How robust is the weakening of the pacific walker circulation in CMIP5 idealized transient climate simulations? *J. Clim.* **31**, 81–97 (2018).
26. Sohn, B. J., Yeh, S.-W., Schmetz, J. & Song, H.-J. Observational evidences of Walker circulation change over the last 30 years contrasting with GCM results. *Clim. Dyn.* **40**, 1721–1732 (2012).

27. Lindzen, R. S. & Nigam, S. On the role of sea surface temperature gradients in forcing low-level winds and convergence in the tropics. *J. Atmos. Sci.* **44**, 2418–2436 (1987).
28. Vergados, P., Ao, C. O., Mannucci, A. J. & Kursinski, E. R. Quantifying the tropical upper tropospheric warming amplification using radio occultation measurements. *Earth Space Sci.* **8**, e2020EA001597 (2021).
29. Knutson, T. R. & Manabe, S. Time-mean response over the tropical Pacific to increased C02 in a coupled ocean-atmosphere model. *J. Clim.* **8**, 2181–2199 (1995).
30. Heede, U. K., Fedorov, A. V. & Burls, N. J. Time scales and mechanisms for the tropical Pacific response to global warming: a tug of War between the ocean thermostat and Weaker Walker. *J. Clim.* **33**, 6101–6118 (2020).
31. Held, I. M. & Soden, B. J. Robust responses of the hydrological cycle to global warming. *J. Clim.* **19**, 5686–5699 (2006).
32. Fedorov, A. V. & Burls, N. J. What controls the mean east–west sea surface temperature gradient in the equatorial Pacific: the role of cloud Albedo. *J. Clim.* **27**, 2757–2778 (2014).
33. Clement, A. C., Seager, R., Cane, M. A. & Zebiak, S. E. An ocean dynamical thermostat. *J. Clim.* **9**, 2190–2196 (1996).
34. Heede, U. K. & Fedorov, A. V. Eastern equatorial Pacific warming delayed by aerosols and thermostat response to CO_2 increase. *Nat. Clim. Change* **11**, 696–703 (2021).
35. Seager, R. et al. Strengthening tropical Pacific zonal sea surface temperature gradient consistent with rising greenhouse gases. *Nat. Clim. Change* **9**, 517–522 (2019).
36. Bony, S. et al. Robust direct effect of carbon dioxide on tropical circulation and regional precipitation. *Nat. Geosci.* **6**, 447–451 (2013).
37. Jeevanjee, N. Three rules for the decrease of tropical convection with global warming. *J. Adv. Model. Earth Syst.* **14**, e2022MS003285 (2022).
38. Jenney, A. M., Randall, D. A. & Branson, M. Understanding the response of tropical ascent to warming using an energy balance framework. *J. Adv. Model. Earth Syst.* **12**, e2020MS002056 (2020).
39. Silvers, L. G., Reed, K. A. & Wing, A. A. The Response of the large-scale tropical circulation to warming. *J. Adv. Model. Earth Syst.* **15**, e2021MS002966 (2023).
40. Betts, A. K. Climate-convection feedbacks: some further issues. *Clim. Change* **39**, 35–38 (1998).
41. Kociuba, G. & Power, S. B. Inability of CMIP5 models to simulate recent strengthening of the Walker circulation: implications for projections. *J. Clim.* **28**, 20–35 (2015).
42. Li, G. & Ren, B. Evidence for strengthening of the tropical Pacific Ocean surface wind speed during 1979–2001. *Theor. Appl. Climatol.* **107**, 59–72 (2011).
43. Bordbar, M. H., Martin, T., Latif, M. & Park, W. Role of internal variability in recent decadal to multidecadal tropical Pacific climate changes. *Geophys. Res. Lett.* **44**, 4246–4255 (2017).
44. DiNezio, P. N., Vecchi, G. A. & Clement, A. C. Detectability of changes in the Walker circulation in response to global warming*. *J. Clim.* **26**, 4038–4048 (2013).
45. Han, W. et al. Decadal variability of the Indian and Pacific Walker cells since the 1960s: do they covary on decadal time scales? *J. Clim.* **30**, 8447–8468 (2017).
46. Kosaka, Y. & Xie, S. P. Recent global-warming hiatus tied to equatorial Pacific surface cooling. *Nature* **501**, 403–407 (2013).
47. Luo, J. J., Sasaki, W. & Masumoto, Y. Indian ocean warming modulates Pacific climate change. *Proc. Natl Acad. Sci. USA* **109**, 18701–18706 (2012).
48. Power, S. B. & Kociuba, G. What caused the observed twentieth-century weakening of the Walker circulation? *J. Clim.* **24**, 6501–6514 (2011).
49. Zhang, L. et al. Indian ocean warming trend reduces pacific warming response to anthropogenic greenhouse gases: an inter-basin thermostat mechanism. *Geophys. Res. Lett.* **46**, 10882–10890 (2019).
50. Chung, E.-S. et al. Reconciling opposing Walker circulation trends in observations and model projections. *Nat. Clim. Change* **9**, 405–412 (2019).
51. Collins, M. et al. The impact of global warming on the tropical Pacific ocean and El Niño. *Nat. Geosci.* **3**, 391–397 (2010).
52. Heede, U. K. & Fedorov, A. V. Colder eastern equatorial pacific and stronger Walker circulation in the early 21st century: separating the forced response to global warming from natural variability. *Geophys. Res. Lett.* **50**, e2022GL101020 (2023).
53. Watanabe, M., Iwakiri, T., Dong, Y. & Kang, S. M. Two competing drivers of the recent Walker circulation trend. *Geophys. Res. Lett.* **50**, e2023GL105332 (2023).
54. Kang, S. M., Shin, Y., Kim, H., Xie, S. P. & Hu, S. Disentangling the mechanisms of equatorial Pacific climate change. *Sci. Adv.* **9**, eadf5059 (2023).
55. Watanabe, M. et al. Possible shift in controls of the tropical Pacific surface warming pattern. *Nature* **630**, 315–324 (2024).
56. Kim, H., Kang, S. M., Kay, J. E. & Xie, S. P. Subtropical clouds key to southern ocean teleconnections to the tropical Pacific. *Proc. Natl Acad. Sci. USA* **119**, e2200514119 (2022).
57. Cai, W. et al. Increased ENSO sea surface temperature variability under four IPCC emission scenarios. *Nat. Clim. Change* **12**, 228–231 (2022).
58. Chen, L., Li, T., Yu, Y. & Behera, S. K. A possible explanation for the divergent projection of ENSO amplitude change under global warming. *Clim. Dyn.* **49**, 3799–3811 (2017).
59. Riahi, K. et al. The shared socioeconomic pathways and their energy, land use, and greenhouse gas emissions implications: an overview. *Glob. Environ. Change* **42**, 153–168 (2017).
60. Eyring, V. et al. Overview of the coupled model intercomparison project phase 6 (CMIP6) experimental design and organization. *Geosci. Model Dev.* **9**, 1937–1958 (2016).

Acknowledgements

This study is jointly supported by the National Natural Science Foundation of China under grant nos. 42125502, 42305027, and the National Key Research and Development Program of China (2020YFA0608904). M.W. is supported by the "CUG Scholar" Scientific Research Funds at China University of Geosciences (Wuhan) (Project No. 2022120). C.L. is supported by the Clusters of Excellence CLICCS (EXC2037), University of Hamburg, funded by the German Research Foundation (DFG). We acknowledge the World Climate Research Program's Working Group on Coupled Modeling, which is responsible for CMIP6, and thank the climate modeling groups for producing and making available the model output. We thank Dr. Lin Chen from Nanjing University of Information Science and Technology for his comments and suggestions on understanding the air-sea feedback processes.

Author contributions

M.W. conceived and designed the study, with support from C.L. M.W. conducted the analysis and drafted the initial manuscript in discussion with C.L. and Z.Z. M.C., H.L., and X.C. provided comments and revised the manuscript. T.Z. contributed to data curation and provided comments. Z.Z. edited the manuscript. All the authors contributed to the scientific interpretation of the results.

Competing interests

The authors declare no competing interests.

Additional information

Supplementary information The online version contains supplementary material available at https://doi.org/10.1038/s41467-024-53509-6.

Correspondence and requests for materials should be addressed to Mingna Wu or Zhongshi Zhang.

Peer review information *Nature Communications* thanks Jun Ying and the other, anonymous, reviewer for their contribution to the peer review of this work. A peer review file is available.